IOPscience iopscience.iop.org

Home Search Collections Journals About Contact us My IOPscience

Selective-area growth of vertically aligned GaAs and GaAs/AlGaAs core–shell nanowires on Si(111) substrate

This content has been downloaded from IOPscience. Please scroll down to see the full text.

2009 Nanotechnology 20 145302

(http://iopscience.iop.org/0957-4484/20/14/145302)

View the table of contents for this issue, or go to the journal homepage for more

Download details:

IP Address: 128.178.120.97
This content was downloaded on 07/06/2016 at 08:32

Please note that terms and conditions apply.

Nanotechnology 20 (2009) 145302 (8pp) doi:10.1088/0957-4484/20/14/145302

Selective-area growth of vertically aligned GaAs and GaAs/AlGaAs core–shell nanowires on Si(111) substrate

Katsuhiro Tomioka[1,3], **Yasunori Kobayashi**[1], **Junichi Motohisa**[1], **Shinjiroh Hara**[2] and **Takashi Fukui**[1,2]

[1] Graduate School of Information Science Technology, Hokkaido University, North 14 West 9, Sapporo 060-0814, Japan
[2] Research Center for Integrated Quantum Electronics (RCIQE), Hokkaido University, North 13 West 8, Sapporo 060-8628, Japan

E-mail: tomioka@rciqe.hokudai.ac.jp

Received 18 December 2008, in final form 23 January 2009
Published 17 March 2009
Online at stacks.iop.org/Nano/20/145302

Abstract
We report on selective-area growth of vertically aligned GaAs nanowires on Si(111) substrate. Modification of the initial Si(111) surface by pretreatment under an AsH_3 atmosphere and low-temperature growth of GaAs were important for controlling the growth orientations of the GaAs nanowire on the Si(111) surface. We also found that the size of openings strongly affected the growth morphology of GaAs nanowires on Si(111). Small diameter openings reduced the antiphase defects and improved the optical properties in the GaAs nanowires. Moreover, we realized coherent growth without misfit dislocation at the GaAs/Si interface. Finally, we demonstrated fabrication of a GaAs/AlGaAs core–shell nanowire array on a Si surface and revealed that the luminescence intensity was markedly enhanced by passivation effects. These results are promising for future III–V nanowire-based optoelectronic integration on Si platforms.

1. Introduction

Semiconductor nanowires (NWs) constitute a pioneering area for nanoelectronic and optoelectronic devices [1–6]. The epitaxy of III–V NWs on Si has especially been attracting a great deal of attention, making it possible to apply them in large-scale integrated circuits (LSIs) because one-dimensional (1D) vertical nanoarchitectures and their fast electron mobility at room temperature are advantageous for achieving high-density integration, low power consumption, and ultrafast electronic devices on Si platforms. Moreover, monolithic integration of electron and photonic devices on Si is expected because almost all III–V compound semiconductors have a direct band gap while Si has an indirect band gap. Thus, studies on the epitaxy of III–V NWs on Si have become increasingly important [7–12]. However, serious problems remain in controlling the growth directions of III–V NWs and their alignment on Si. The growth direction of NWs is closely related to the nature of the growth of polar materials on non-polar Si. That is, most III–V NWs with a zinc-blende crystal structure preferentially grow along the $\langle 111 \rangle B$ or $\langle 111 \rangle A$ directions [13–15], which enables us to fabricate vertically free-standing NWs on $(111)B$ or $(111)A$ oriented III–V substrates. For Si substrates, however, the (111) surface is non-polar and there are no distinctions between A and B planes. Thus, growth in four equivalent $\langle 111 \rangle$ growth directions of III–V NWs always occurs on the Si(111) substrate; one of these directions is perpendicular to the Si(111) surface and the three others are tilted to the (111) surface. This results in the formation of NWs inclined to the (111) surface, which is not advantageous for attaining high-density integration of NW-based devices on Si.

In the previous study, this problem was overcome with appropriate termination of the surface and demonstrated by the direction- and site-controlled growth of InAs NWs on Si [16]. In this paper, we further advanced this approach into rational integration of other III–V NWs on Si, and achieved a position-controlled and vertically aligned GaAs NW array on

[3] Author to whom any correspondence should be addressed.

 © 2009 IOP Publishing Ltd Printed in the UK

Si substrates by using selective-area metal–organic vapor phase epitaxy (SA-MOVPE). GaAs is an ideal and well-developed material for light-emitting-diodes, lasers and photo-diodes, with GaAs-related alloys. Once we can directly fabricate GaAs NWs on Si, we can heterogeneously integrate such optical devices into the NWs on Si.

The results of micro-Raman scattering revealed that the TO and LO phonon spectra of grown NWs were the same as those of GaAs and the NWs had no strain that resulted from lattice mismatch. The transmission electron microscopy (TEM) images indicated that the crystallographic structure of thin GaAs NWs was composed of zinc-blende (ZB) and wurtzite (WZ) with a short period of transition thickness. Studies of SEM and photoluminescence (PL) revealed that the size of the mask openings played an important role in the initial nucleation process and formation of the NWs. Coherent growth without misfit dislocation was particularly confirmed at the heterointerface of GaAs and Si for NWs with small diameters. In addition, GaAs/AlGaAs core–shell NW arrays were also fabricated on Si, and these revealed that the PL intensity was drastically enhanced compared with that of GaAs NWs on Si because the surface states of GaAs NWs are passivated with AlGaAs shell layers.

2. Experimental details

The n-type (111)-oriented Si substrates were used for the starting substrates. First, the substrates were etched with hydrofluoric (HF) solution and cleaned by so-called RCA cleaning with SC1 and SC2 solutions ($1NH_4OH:1H_2O_2:5H_2O$ and $1HCl:1H_2O_2:6H_2O$ at 75 °C) to remove metal particles from their surfaces. Then, 20 nm thick SiO_2 was formed by using a thermal oxidation process at 950 °C. The formation of SiO_2 at high temperature is a one of the important processes for selective-area growth of III–V on Si to avoid heat shrinkage of the SiO_2 template. Next, the periodic opening patterns were formed on the SiO_2-formed Si surface using electron-beam lithography and wet chemical etching. The opening diameters, d_0, ranged from 50 to 600 nm. Finally, the partially masked substrates were degreased in organic solvents in an ultrasonic bath, and slightly etched with buffered HF (BHF) solution for 3 s to remove native oxide that had formed on the opening area during these processes.

The GaAs growth was carried out using a low-pressure (0.1 atm) horizontal-reactor MOVPE system. The carrier gas used for this growth was hydrogen (H_2) that was purified through Pd film. The total flow rate of the gases was maintained at 5.75 standard liters per minute (SLM). The group III-atom precursor was trimethylgallium (TMGa), trimethylaluminium (TMAl), and the group V-atom precursor was 5% hydrogen-diluted arsine (AsH_3) gas. The GaAs was grown at 750 °C for 60 min. The partial pressure of TMGa was 1.0×10^{-6} atm and that of AsH_3 was 2.5×10^{-4} atm. The AlGaAs was grown at 730 °C for 10 min. The partial pressures of TMGa, TMAl, and AsH_3 were 8.6×10^{-7}, 5.0×10^{-7}, and 1.3×10^{-4} atm, respectively.

Prior to growth, thermal cleaning in an H_2 ambient was carried out at 925 °C to remove the native oxide that had formed on the opening areas of the masked substrates when transferring the samples into the reactor. Approximately 1 nm thick native oxide was formed on the opened patterns, and the oxide disrupted selective-area growth.

High-resolution TEM images were acquired using a transmission electron microscope (HITACHI H-9000UHR). The acceleration voltage was 300 kV. The incident electron beam was along the $\langle\bar{1}10\rangle$ direction. The samples were sliced into thin sections by using focused-ion-beam (FIB) and Ar-ion-milling techniques. Raman scattering measurements were conducted to confirm that the materials grown on the Si were those that we had designed and there was strain in the NWs. An He–Ne laser, whose wavelength was 632.8 nm, was focused on an approximately 2 μm spot on the substrates with the NWs grown on them. The laser power was about 0.1 mW. The incident direction of the excitation light was along the $\langle 111\rangle B$ direction in the (111) backscattering geometry. Microphotoluminescence (μ-PL) was obtained at 4 K. The excitation light was an He–Ne laser, which was focused on an approximately 2 μm spot on the substrate. Approximately 10 NWs were included in the spot.

The image calculation process was as follows. First, we derived a series of $\langle\bar{1}11\rangle$ reciprocal lattice spots from fast Fourier transform (FFT) patterns of a high-resolution TEM image. Second, we transformed the derived FFT patterns into real images by inverse FFT. After this process, only $(111)A$ planes appeared in the inverse FFT image as white lines. The separation of the lines at the Si substrate was approximately 3.32 Å in the $\langle\bar{1}\bar{1}2\rangle$ direction.

3. Results and discussion

3.1. Selective-area growth of vertically aligned GaAs nanowires on Si

The selective-area MOVPE method uses patterned amorphous thin films as mask templates and the growth mechanism progresses via a facet-growth mechanism without catalysts. We used 20 nm thick SiO_2 films with circular-opening patterns for the templates on Si(111) as previous reported [16], and GaAs was grown following the sequence summarized in figure 1(a) to fabricate vertical GaAs NWs on the Si(111) surface.

First, *in situ* thermal cleaning (T.C.) was carried out at 925 °C. The *in situ* T.C. was done to remove native oxides from the opening regions, which disrupts the nucleation process of GaAs. The high-temperature annealing also alters the surface reconstruction of Si(111) as well as decomposing SiO_2. This involves a process to modify the Si(111) surface into $(111)B$-like oriented planes prior to GaAs NW growth, which is a step necessary for accomplishing vertical NW growth on Si [16] because the growth direction of GaAs NWs is always in the $\langle 111\rangle B$ direction. When the temperature is raised above 830 °C, a 7×7 reconstructed (111) surface is transformed into a stable Si(111) 1×1 reconstructed surface. After the Si(111) 1×1 surface is reconstructed, metastable surface reconstructions, such as $c2 \times 4$, $c2 \times 8$, $\sqrt{3} \times \sqrt{3}$, are formed during cooling from high temperatures

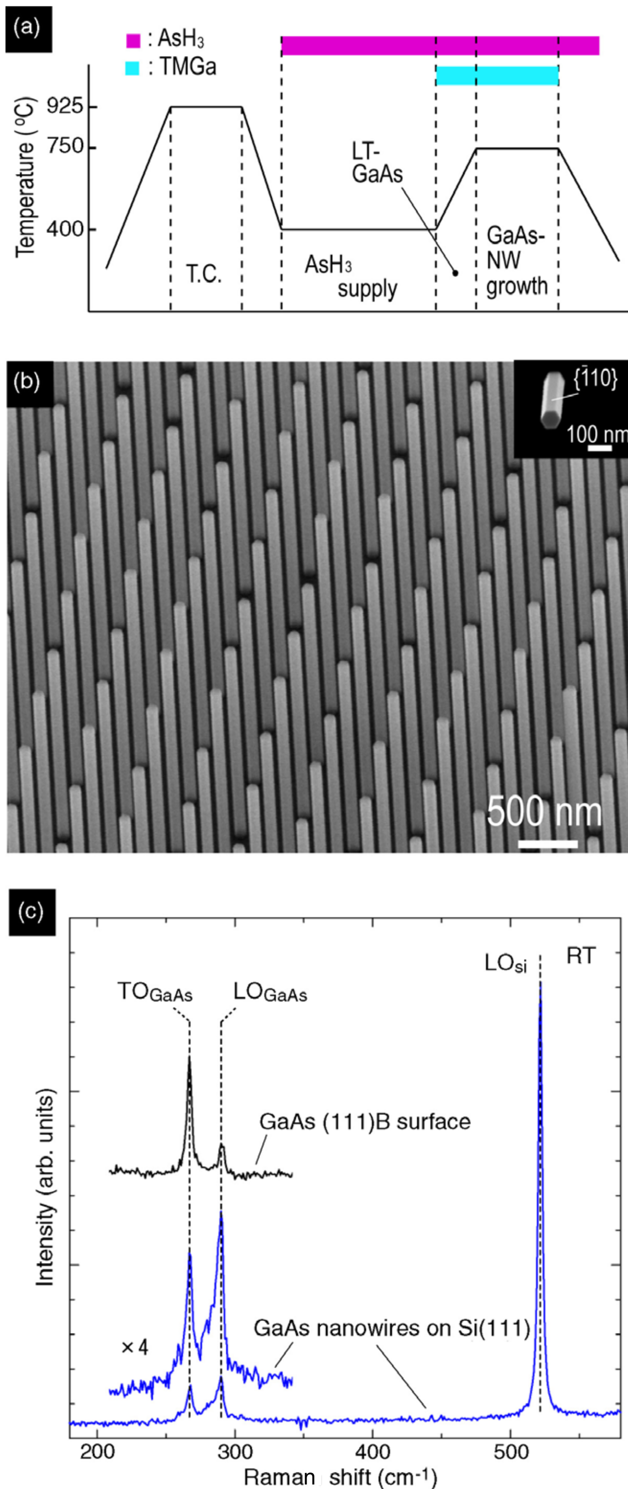

Figure 1. (a) Growth sequence for GaAs NWs grown on Si(111) substrate. T.C. stands for thermal cleaning and LT means low temperature. (b) 45°-tilted view of a scanning electron microscopy (SEM) image of a GaAs NW array on a Si(111) surface. (c) μ-Raman spectra of GaAs NWs measured at room temperature (RT).

to 400 °C [17–19]. We should note that the growth temperature windows for growing III–V semiconductors are mostly within the range of the formation of metastable reconstructions. Such metastable surface reconstructions are thought to randomize the orientation of dangling bonds and/or to disrupt the uniform nucleation process of III–V growth on the Si surface. Thus, the cooling process was done in a hydrogen (H_2) ambient followed by AsH_3 treatment to form the As-adsorbed Si(111)1 × 1 surface [Si(111)1 × 1:As]. This surface corresponds to the (111)B-oriented surface because the topmost Si atoms are substantially replaced by As atoms. Next, a thin GaAs low-temperature (LT) buffer layer was grown during temperature changes from 400 to 750 °C. This sequence took 3 min. This growth process is important for preventing the thermal desorption of As atoms from the Si surface because the As–Si bonding strength is weak at high temperature.

Following all these steps, GaAs NWs could be grown in the vertical [111] direction on Si as shown in figure 1(b). The yield of the vertically aligned GaAs NWs was 100%. The grown NWs had a hexagonal cross-section having a (111)B top surface and {$\bar{1}$10} sidewall facets. The GaAs NWs in figure 1(b) measured 70 nm in diameter, and 1.7 μm in height. The standard deviation in diameter fluctuations was ±3 nm in this case. The NW diameters were almost equal to that of the mask openings (d_0), which means that lateral overgrowth in the ⟨$\bar{1}$10⟩ directions was completely suppressed because of As desorption on the {$\bar{1}$10} sidewalls. Figure 1(c) shows the Raman spectra for GaAs NWs. LO and TO phonon peaks can be observed as well as an Si LO phonon peak. Neither LO or TO phonons indicate a peak shift with respect to the GaAs bulk case. This means that the grown NWs on Si are pure GaAs without strains resulting from large lattice mismatch.

3.2. *Crystallographic structure of thin GaAs nanowire*

Figure 2(a) shows a cross-sectional TEM image of a GaAs NW with a diameter of 27 nm. The growth direction of GaAs NW is normal to the Si(111) surface. This indicates that the chemical structure of the Si(111) surface develops into a (111)B-like orientation as expected. The inset of figure 2(a) shows the top of the typical NW. The TEM images near the tops of five NW specimens were checked and no catalysts were observed on top surfaces of the NWs. This means that the GaAs NW growth in this case differs from both vapor–liquid–solid mechanisms and self-catalyzed growth [20].

Figure 2(a) also shows that the GaAs NW contains a short period of rotational twins in the growth direction. Rotational twins as well as intrinsic and extrinsic stacking faults generated from the slipped (111) plane to the ⟨$\bar{1}\bar{1}$2⟩ directions usually form wurtzite (WZ) configurations along the ⟨111⟩ stacking direction in a ZB structure. As rotational twins were observed for GaAs NWs grown on GaAs(111)B substrate [21], the formation of twins is not specific to the NWs on Si. According to statistical analysis of the transition thickness of ZB or WZ [22], the distribution of transition thickness is almost within three monolayers (MLs) as shown in figure 2(b). This indicates that the occurrence frequency of rotational twins is within three MLs. Also, the fraction of the ZB segment is 53%, and that of the WZ segment is 47%, which means that the NW is bistable in forming ZB and WZ structures. The selected-area electron diffraction (SAED) pattern in figure 2(c)

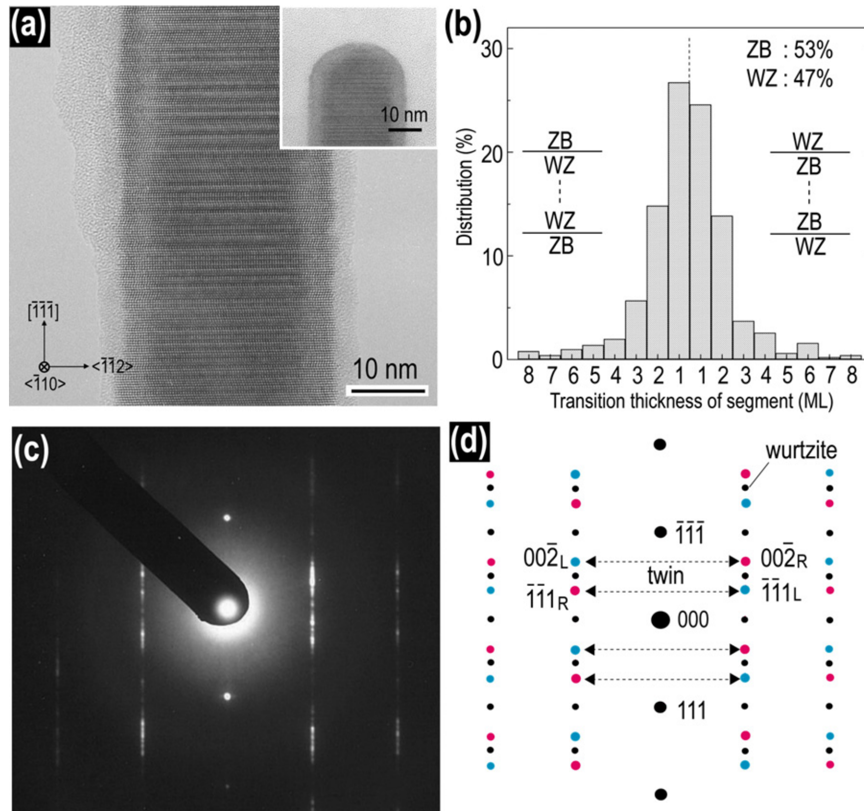

Figure 2. (a) TEM image of a GaAs NW grown on Si(111). The diameter is 27 nm. The inset shows the top of the GaAs NW on Si. (b) Statics of the thickness of the transition from zinc-blende (ZB) to wurtzite (WZ), and vice versa, in NWs. (c) Selected-area electron diffraction (SAED) pattern of a GaAs NW. (d) Illustration of a simulated diffraction pattern including zinc-blende, its twin, and the wurtzite configuration.

shows that the WZ configuration as well as that of the ZB with twins is superimposed with the diffraction patterns seen in figure 2(d). Furthermore, unusual Bragg spots that are neither from twinned ZB nor from WZ can be observed in figure 2(c); however, they can reasonably be explained by the diffraction spots of 4H or 6H polytype structures. Such short periods reflecting rotational twins and 4H- or 6H-like spots have been previously observed in InAs NWs on InAs substrate, leading to the formation of structures close to formation of 4H or 6H polytypes [22]. Thus, a similar structure was formed for the present GaAs NW.

According to a simulation of NW structure based on the Monte Carlo method with empirical potentials [23], the average period of the WZ segment in III–V NWs is independent of the diameter in a range from 10 to 80 nm and a small number of nuclei lead to a shorter period of WZ segments. This was consistent with our previous results on InAs NWs. However, for GaAs NWs, the period of the WZ segments depends on the NW size because GaAs NWs with larger diameters of around 200 nm revealed that their Bragg spots were equal to the value in the simulation as shown in figure 2(d) [21]. This phenomenon only seemed to be observed for thin GaAs NWs. The dependence of the average period of WZ segments on size for GaAs NWs will be reported separately.

3.3. Size dependence of openings

The GaAs NW growth was investigated for different opening areas to obtain insights into the process of nucleation of GaAs on Si(111). Figure 3(a) shows a plan view of an SEM image of planar GaAs growth on $(111)B$-oriented Si(111), which was formed by using the sequence in figure 1(a). We can see numerous triangle-shaped three-dimensional (3D) islands and their coalescence. The Si(111) surface has been modified to a $(111)B$-like surface using the specific sequence. The triangular shapes reflect a threefold symmetry for the $(111)B$ surface and the orientation of the facet of the 3D islands is what one would expect from the symmetry. However, 30°-rotated 3D islands, which are reflective of the symmetry of 3D islands across the $\{1\bar{1}0\}$ plane, can also be observed in figure 3(a). Since the initial nucleation process for the 3D GaAs islands on the $(111)B$-like Si surface is assumed to be based on the coalescence of triangular two-dimensional (2D) islands, as illustrated in figure 3(e), the growth results shown in figure 3(a) suggest that the rotational twins are introduced in the early stages of initial nucleation. Moreover, the coalescence of 2D islands with the rotational twins results in the generation of 3D islands with antiphase defects (or domains) in several parts of the boundary with coalescence. This is unavoidable as long as the nucleation process is dominated by the coalescence of multiple 3D islands. Similar phenomena can also be observed for selective-area growth when the openings are

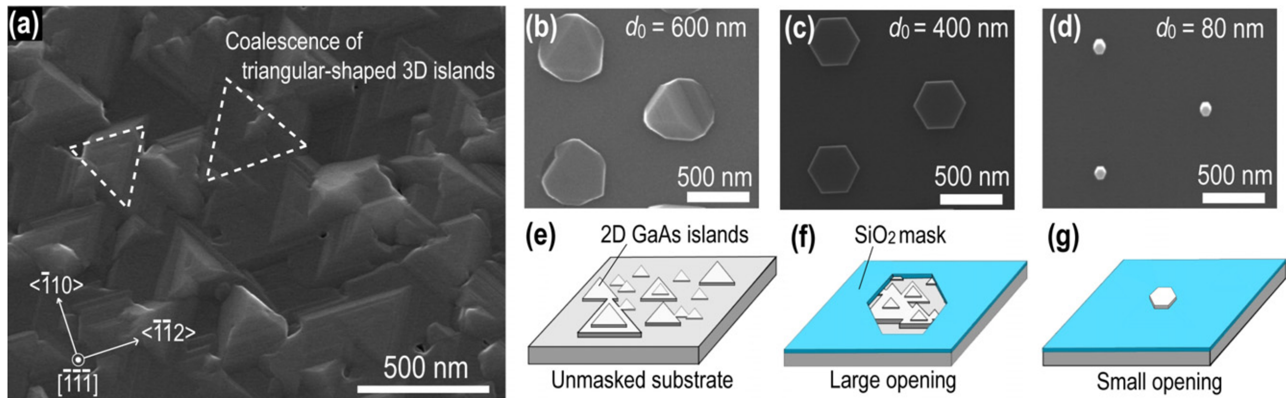

Figure 3. (a) Plan view of GaAs planar growth on Si(111) substrate. Dashed red triangles represent two-dimensional (2D) islands. Plan view of SEM images of GaAs growth on masked Si(111): (b) the diameter of the openings, d_0, was 600 nm. (c) $d_0 = 400$ nm and (d) $d_0 = 80$ nm. (e) Illustration of nucleation of 2D islands and its coalescence on unmasked Si(111) surface. Illustration of growth behavior of GaAs: (f) large opening and (g) small opening on masked Si(111) surfaces.

large, as shown in figures 3(b) and (f). Here, d_0 was 600 nm in diameter and hillock-like structures surrounded with unexpected facets were formed on the openings. This is because a tremendous amount of coalescence occurred on the relatively large surface areas, and formed many steps and kinks within the openings. The roughness seemed to form unexpected facets on some parts of their surface, and the structures did not differ from the planar GaAs shown in figure 3(a). The hexagonal columns surrounded with the $\{\bar{1}10\}$ vertical sidewall facets and the $(111)B$ top surface, on the other hand, could be formed on smaller openings, as shown in figures 3(c) and (d) corresponding to $d_0 = 400$ and 80 nm. For $d_0 = 400$ nm, there were partly hillock-shaped structures similar to those in figure 3(b) on some parts of the openings, but they are completely suppressed for $d_0 = 80$ nm. Therefore, we concluded that the sizes of openings, which determined the number of 2D islands in the initial nucleation process, were important for growing GaAs NWs on the Si surface in SA-MOVPE.

The effect of the size of the openings was further confirmed with micro-PL (μ-PL) measurements and the quality of NWs, as summarized in figure 4. The excitation laser spot for the μ-PL was 2 μm in diameter, and the pitch of the NW array was 600 nm. Thus, approximately 10 NWs were included in the excitation area. Two main luminescence bands were observed from the GaAs grown on the planar region of Si as well as GaAs NWs on Si. The first is the near band-edge emission at around 1.51 eV, and the second is the deep-level-related emission at around 1.33 eV. The emission is very weak and dominated by deep-level-related recombination for planar GaAs growth on Si, while strong near band-edge emissions were observed for GaAs NWs grown on Si, especially for $d = 70$ nm. This difference is thought to be due to the number of non-radiative recombination centers in grown materials. That is, a number of non-radiative recombination centers are generated in planar GaAs presumably because of dislocations caused by large mismatch in the lattice constant and the thermal expansion coefficient. Also, antiphase defects generated in the boundary of coalescent 3D islands, part of which contains twins, lead to the deep-level-related emissions. The deep-level-related PL emissions are still dominant for $d_0 = 400$ nm, as shown in figure 4(c), which implies that they still contain many antiphase defects originating from the coalescence of 2D and 3D islands, although their geometrical shape is in the form of a smooth top surface and facet sidewalls as already shown in figure 3(c). However, the stronger near band-edge PL emissions in GaAs NWs on Si indicate that radiative recombination becomes much more efficient than

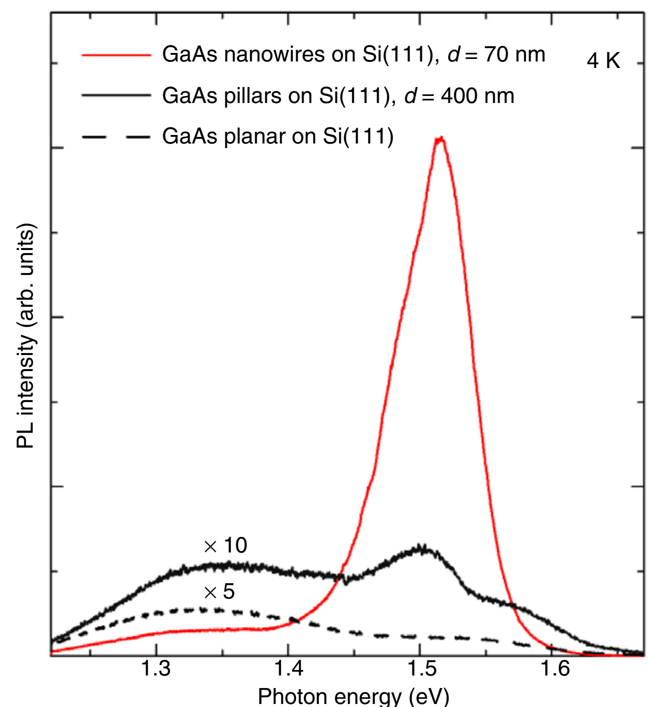

Figure 4. Optical properties of GaAs NWs on Si(111). μ-PL spectra of a GaAs NW array on Si. The solid red line represents GaAs NWs on Si(111) whose diameter (d) is 70 nm, the solid black line represents the GaAs pillar on Si(111) whose d is 400 nm, and the broken line represents planar GaAs grown on the $(111)B$-oriented Si(111) surface.

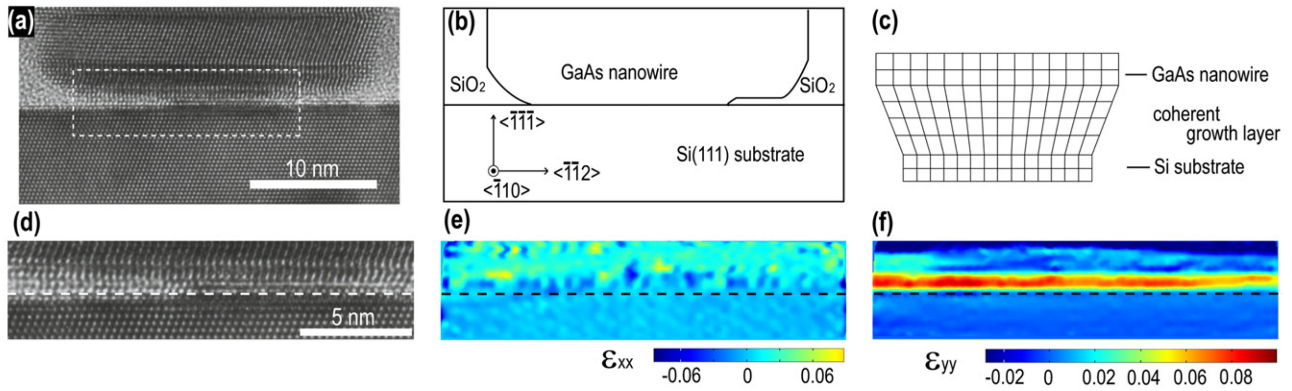

Figure 5. (a) Cross-sectional TEM image of a GaAs NW grown on Si(111). The NW diameter is 27 nm. The dashed rectangle shows the region of the heterojunction of GaAs and Si(111), which was 19 nm in diameter. (b) Illustration of the TEM image of (a). (c) Description of coherent epitaxial growth. (d) Magnified image of the dashed rectangle in (a). (e) ε_{xx} strain mapping calculated from image (d). The standard value for calculation is the lattice constant of Si in the $\langle\bar{1}\bar{1}2\rangle$ direction, i.e., $a_{\mathrm{Si}(x)} = 3.328$ Å. (f) ε_{yy} strain mapping estimated from image (d). The standard value for calculation is the lattice constant of Si in the vertical $\langle 111\rangle$ direction, i.e., $a_{\mathrm{Si}(y)} = 3.136$ Å.

that of planar GaAs on Si and this is ascribed to the limited number of initial nucleation of 2D islands and the elimination of antiphase defects.

Photoluminescence for GaAs NWs grown on Si(111) shows broad asymmetric spectra at around 1.51 eV, which means that the PL spectra result from several optical transitions as well as interband transitions, such as free-exciton and carbon-related donor–acceptor pair transitions. The full widths at half-maximum (FWHM) of all luminescence centers are several tens of meV. The slightly large FWHM in the PL spectra are commonly observed for homoepitaxial GaAs NWs [24]. Although the origin of the broadened PL bands in NWs is still unclear, the optical properties in thin GaAs NWs on Si are found to be less effective with some defects due to lattice mismatch and coalescence.

3.4. Morphology of the heterointerface of GaAs and Si

It should be noted that the above results do not imply a complete removal of misfit dislocations. Detailed analysis of TEM images revealed that NWs in some cases are grown coherently even with the lattice mismatch. Figure 5(a) shows a TEM image of a heterointerface of a GaAs NW and Si substrate. SiO_2 was observed at the edge of the heterointerface of GaAs and Si, as illustrated in figure 5(b). This originated from the tapered sidewalls of the SiO_2 masks, which are formed due to the isotropic nature of the etching with HF solutions. Thus, the actual opening diameter of the heterointerface is 19 nm (dashed rectangle in figure 5(a))[4]. The magnified image of the heterointerface in figure 5(d) reveals that the GaAs is epitaxially grown on the Si(111) surface. The number of (111)A planes in the GaAs NW measured using the FFT technique is the same as that of (111) planes in the mask opening of the Si substrate (54 planes; see section 2). This means that coherent growth occurs without any misfit dislocations, as schematically shown in figure 5(c).

Strain mappings estimated from displacement of bright spots in the TEM image are shown in figures 5(e) and (f). Here, the strains, ε_{xx} and ε_{yy}, were calculated from the displacement of bright spots in figure 5(d) by using a peak-pair-finding algorithm [25] and the displacements of the bright spots are defined by $u_{xx} = \Delta x - a_{\mathrm{Si}(x)}$ for the in-plane $\langle\bar{1}\bar{1}2\rangle$ direction and $u_{yy} = \Delta y - a_{\mathrm{Si}(y)}$ for the vertical $\langle 111\rangle$ direction. Δx and Δy are the displacements of the bright spots for each direction. $a_{\mathrm{Si}(x)}$ and $a_{\mathrm{Si}(y)}$ correspond to the lattice constants in the in-plane and vertical directions of the Si substrate estimated from the TEM image. Also the strains ε_{xx} and ε_{yy} are determined from $\varepsilon_{xx} = \partial u/\partial x$ and $\varepsilon_{yy} = \partial u/\partial y$, where u is $\sqrt{u_{xx}^2 + u_{yy}^2}$. Note that, since the displacement of the atoms is calculated on the basis of the position of the atoms in crystalline Si, unstrained GaAs is mapped into a layer with a strain of +4.1% in the definition. The error in the strain calculation is approximately ±0.5%. Strains ε_{xx} in figure 5(e) were calculated to be very small in the first four MLs of a GaAs NW from the heterojunction and close to the value calculated for the Si substrate. This indicates that the lattice constant of GaAs in the $\langle\bar{1}\bar{1}2\rangle$ direction in the four-ML region is consistent with that of Si and the region has compressive strain. The ε_{yy} strain mapping of GaAs NW, on the other hand, shows lamellar tensile strain in the four-ML region, and the amount is far larger than 4.1%. The misfit strain, ε_{yy}, estimated from the lattice mismatch and elastic stiffness is +3.7% when ε_{xx} has compressive strain at −4.1%. The estimated ε_{yy} becomes approximately +7.9% because the calculation of the mapping is based on $a_{\mathrm{Si}(y)}$. This estimate is almost consistent with the value for lamellar tensile strain in figure 5(f). This means that the lattice constant of GaAs NW in the $\langle 111\rangle$ direction is increased at the heterointerface. Thus, a transient layer with compressive strain in the in-plane direction and tensile strain in the vertical direction compensates for the lattice mismatch. This concludes the section on why GaAs NWs grow coherently on the Si(111) substrate, as shown in figure 5(c), regardless of lattice mismatch.

[4] This specimen was thinned with FIB and Ar-ion-milling methods. The specimen was finally thinned to 70 nm. Because it was thicker than the GaAs NW, an image of the amorphous SiO_2 was superimposed on the image at the heterointerface. Although this led to extra bright contrast at the interface, it can still be distinguished in the lattice image.

In contrast to the case for our previous report on InAs NW growth on Si [16], periodic strains due to misfit dislocations cannot be observed in figures 5(e) and (f). This is probably because the lattice mismatch in the GaAs/Si system is smaller than that in the InAs/Si system, and that opening diameter, d_0, is sufficiently small for coherent NW growth. According to the calculations by Ertekin *et al* [26] and Glas [27], the critical diameter for coherent NW growth is around 40 nm in the case of the GaAs/Si system (the lattice mismatch is about 4.1%). Experimental results shown in figure 5 are within the theoretical coherent growth region. It should be noted that GaAs NWs with a larger diameter ($d\rangle$40 nm) are also formed that are extremely uniform, as shown in figure 1(b), and the results of Raman scattering, shown in figure 1(c), indicated the absence of strains. It is still not clear whether those NWs contain misfit dislocations at the interface. However, antiphase defects with the coalescence of nucleation as discussed below are thought to be less effective for GaAs NWs with 70 nm diameters. Further investigations are required to clarify the boundary between coherent and incoherent growth as a function of d_0 to apply NWs in some devices on Si.

3.5. Fabrication of a GaAs/AlGaAs core–shell nanowire array on Si

The GaAs/AlGaAs core–shell NWs on the Si(111) surface were grown as schematically illustrated in figure 6(a). Core–shell structures in NWs are useful for *in situ* passivation against surface states and they are suited for applications and optical devices based on GaAs NWs because bare GaAs NWs have many surface states on their large surface area that lead to a non-radiative recombination process and surface depletion. In addition, growth of an AlGaAs shell layer is superior to the method of surface passivation using chemicals such as $(NH_4)_2S$ solution [28] because of its chemical stability in ambient. The growth direction with the SA-MOVPE method can be controlled radially or axially by controlling the growth temperature. The details for this selectivity of growth directions have been reported previously [29, 30]. Figure 6(b) shows a SEM image of the vertical GaAs/AlGaAs core–shell NWs grown on Si(111). The AlGaAs layer was grown at 730 °C for 10 min. The V/III ratio was 90. The diameter of the NWs during AlGaAs growth increased from 75 to 150 nm, while the heights of the NWs remained constant to 1.75 μm. This means that the AlGaAs layer only grew radially, i.e., in the $\langle\bar{1}10\rangle$ directions. The lateral-growth rate of the AlGaAs was 7.5 nm min^{-1}. The μ-PL spectra of the GaAs/AlGaAs core/shell NWs are shown in figure 6(c). The PL intensity of the core/shell NWs is dramatically enhanced (490×) compared to that of the GaAs NWs on Si. This indicates that the AlGaAs shell layer acted as a passivation layer to reduce the surface non-radiative recombination centers in GaAs NWs. This suggests that shell-layer growth is also useful for *in situ* passivation of NWs and their applications to Si platforms.

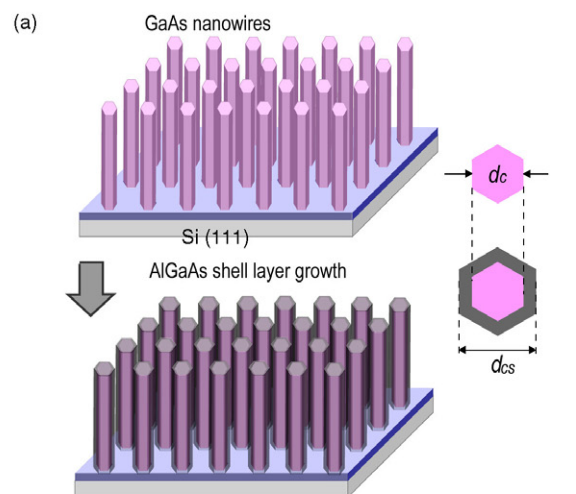

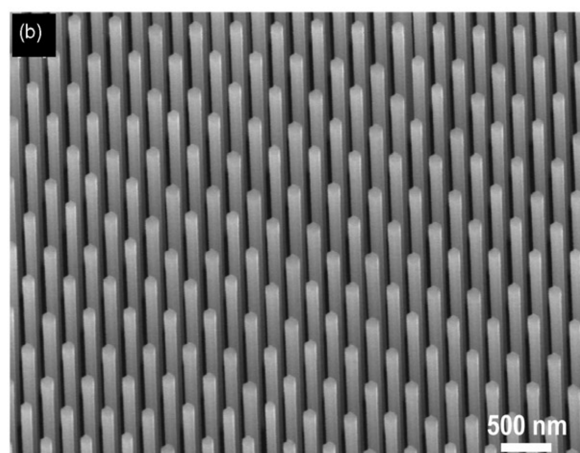

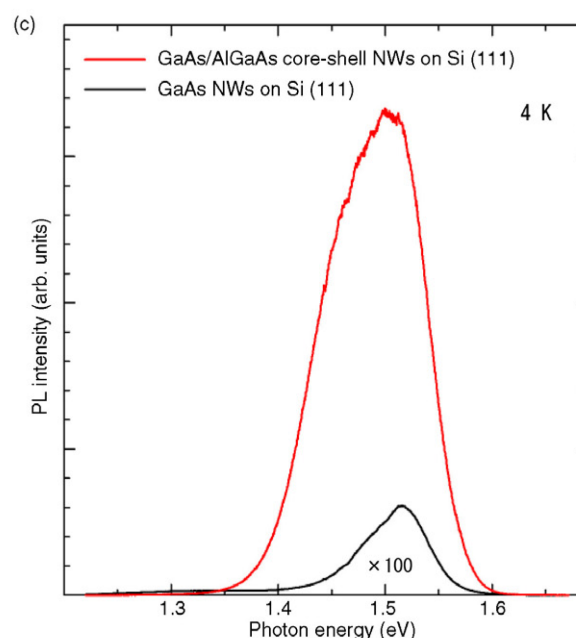

Figure 6. (a) Schematic illustration of GaAs NWs before and after growth of AlGaAs shell layer. Insets indicate the diameters of both NWs. d_c is the diameter of the core GaAs NW, and d_{cs} means that of the core/shell NW. (b) 30°-tilted view of a GaAs/AlGaAs core–shell NW array on Si(111) substrate. (c) μ-PL spectra of NWs. The orange solid line shows GaAs/AlGaAs core–shell NWs on Si(111). The black line shows GaAs NWs on Si(111). Spectra were acquired at 4 K.

4. Summary

Vertically aligned GaAs and GaAs/AlGaAs core–shell NW arrays have been successfully integrated with Si(111) surface by using selective-area MOVPE. Effective processes for forming vertical GaAs NWs on Si were modifying the Si(111) to a $(111)B$-oriented surface at low temperature (LT) and LT GaAs growth as the temperature is rising. The area of initial nucleation and its coalescence, which could form a flat surface, and the $(111)B$ orientation, on Si(111), to the GaAs growth were also found to be important factors for GaAs NW growth on Si. The μ-PL spectra revealed that using SA-MOVPE to grow GaAs NWs on Si produced almost the same results as homoepitaxially growing GaAs NWs on GaAs$(111)B$ when the NW size was sufficiently small to eliminate the antiphase. The TEM observation indicated that the crystallographic structure of GaAs NWs was zinc-blende with a short period of rotational twins. The cross-sectional TEM images indicated that coherent growth occurred in the case of small diameters of openings. This study on the growth of GaAs NWs on Si confirmed the effectiveness of the method for preparing a $(111)B$-like surface on Si(111), and in combination with the characterization of their optical properties, led to a much clearer understanding of the nature of growth and device applications of III–V NWs on the Si platform.

Acknowledgments

The authors would like to acknowledge Prof. K Hiruma and Prof. T Hashizume for their fruitful discussion and sharing their insights. We also wish to acknowledge Dr Y Ding for his support in the MOVPE experiment. This work was financially supported by a Grant-in-Aid for Scientific Research from the Ministry of Education, Culture, Sports, Science and Technology (MEXT), Japan. One of the authors (KT) would like to acknowledge the financial support provided by a Research Fellowship from the Japan Society for the Promotion of Science (JSPS).

References

[1] Huang Y, Duan X, Cui Y, Lauhon L J, Kim K-H and Lieber C M 2001 *Science* **294** 1313
[2] Huang M H, Mao S, Feick H, Yan H, Wu Y, Kind H, Weber E, Russo R and Yang P 2001 *Science* **292** 1897
[3] Gudiksen M S, Lauhon L J, Wang J, Smith D C and Lieber C M 2002 *Nature* **415** 617
[4] Lauhon L J, Gudiksen M S, Wang D and Lieber C M 2002 *Nature* **420** 57
[5] Johnson J C, Choi H-J, Knutsen K P, Schaller R D, Yang P and Saykally R J 2002 *Nat. Mater.* **1** 106
[6] Hiruma K, Yazawa M, Katsuyama T, Ogawa K, Haraguchi K, Koguchi M and Kakibayashi H 1995 *J. Appl. Phys.* **77** 447
[7] Bakkers E P A M, Dam J A V, Franceschi S D, Kouwenhoven L P, Kaiser M, Verheijen M, Wondergem H and Sluis P V D 2004 *Nat. Mater.* **3** 769
[8] Mårtensson A T, Svesson C P, Wacaser B A, Larsson M W, Seifert W, Deppert K, Gustafsson A, Wallenberg L R and Samuelson L 2004 *Nano Lett.* **4** 1987
[9] Roest A L, Verheijen M A, Wunnicke O, Serafin S, Wondergem H and Bakkers E P A M 2006 *Nanotechnology* **17** S271
[10] Tateno K, Hibino H, Gotoh H and Nakano H 2006 *Appl. Phys. Lett.* **89** 033114
[11] Park H D, Prokes S M, Twingg M E, Cammarata R C and Gaillot A-C 2006 *Appl. Phys. Lett.* **89** 223125
[12] Ihn S-S, Song J-I, Kim T-W, Leem D-S, Lee T, Lee S-G, Koh E K and Song K 2007 *Nano Lett.* **7** 39
[13] Koguchi M, Kakibayashi H, Yazawa M, Hiruma K and Katsuyama T 1992 *Japan. J. Appl. Phys.* **31** 2061
Duan X and Lieber C M 2000 *Adv. Mater.* **12** 298
Panev N, Persson A I, Skold N and Samuelson L 2003 *Appl. Phys. Lett.* **83** 2238
[14] Bhunia S, Kawamura T, Fujikawa S and Watanabe W 2004 *Physica* E **24** 138
Watanabe Y, Hibino H, Bhunia S, Tateno K and Sekiguchi T 2004 *Physica* E **24** 133
Mohan P, Motohisa J and Fukui T 2005 *Nanotechnology* **16** 2903
[15] Dick K A, Deppert K, Karlsson L S, Wallenberg L R, Samuelson L and Seifert W 2005 *Adv. Funct. Mater.* **15** 1603
Jensen L E, Björk M T, Jeppensen S, Persson A I, Ohlsson B J and Samuelson L 2004 *Nano Lett.* **4** 1961
Tomioka K, Mohan P, Noborisaka J, Hara S, Motohisa J and Fukui T 2007 *J. Cryst. Growth* **298** 644
[16] Tomioka K, Motohisa J, Hara S and Fukui T 2008 *Nano Lett.* **8** 3475
[17] Hattori T, Aiba T, Iijima E, Okube Y, Nohira H, Tate N and Katayama M 1996 *Appl. Surf. Sci.* **104/105** 323
[18] Hofer U, Li L, Ratzlaff G A and Heinz T F 1995 *Phys. Rev.* B **52** 5264
[19] Yang Y N and Williams E D 1994 *Phys. Rev. Lett.* **72** 1862
[20] Jabeen F, Grillo V, Rubini S and Martelli S F 2008 *Nanotechnology* **19** 275711
[21] Motohisa J, Takeda J, Inari M, Noborisaka J and Fukui T 2004 *Physica* E **23** 298
Motohisa J, Noborisaka J, Takeda J, Inari M and Fukui T 2004 *J. Cryst. Growth* **272** 180
Noborisaka J, Motohisa J and Fukui T 2005 *Appl. Phys. Lett.* **86** 213102
[22] Tomioka K, Motohisa J, Hara S and Fukui T 2007 *Japan. J. Appl. Phys.* **46** L1102
[23] Yamashita T, Sano K, Akiyama T, Nakamura K and Ito T 2008 *Appl. Surf. Sci.* **254** 7668
[24] Hua B, Motohisa J, Ding Y, Hara S and Fukui T 2007 *Appl. Phys. Lett.* **91** 131112
[25] Galindo P L, Kret S, Sanchez A M, Laval J-Y, Yáñez A, Pizzaro J, Guerrero E, Ben T and Molina S I 2007 *Ultramicroscopy* **107** 1186
[26] Ertekin E, Greaney P A, Chrzan D C and Sands T D 2005 *J. Appl. Phys.* **97** 114325
[27] Glas F 2006 *Phys. Rev.* B **74** 121302(R)
[28] Sandroff C J, Hegde M S, Farrow L A, Chang C C and Harbison J P 1989 *Appl. Phys. Lett.* **362** 54
[29] Noborisaka J, Motohisa J, Hara S and Fukui T 2005 *Appl. Phys. Lett.* **87** 093109
[30] Ikejiri K, Noborisaka J, Hara S, Motohisa J and Fukui T 2007 *J. Cryst. Growth* **298** 616